Chinese Chemical Letters 34 (2023) 107774

Contents lists available at ScienceDirect

Chinese Chemical Letters

journal homepage: www.elsevier.com/locate/cclet

NH_4^+/K^+-substitution-induced C–F–K coordination bonds for designing the highest-temperature hybrid halide double perovskite ferroelastic

Chang-Feng Wang, Na Wang, Chao Shi, Heng-Yun Ye, Yi Zhang*, Le-Ping Miao*

Chaotic Matter Science Research Center, Department of Materials, Metallurgy and Chemistry, Jiangxi University of Science and Technology, Ganzhou 341000, China

ARTICLE INFO

Article history:
Received 10 July 2022
Revised 9 August 2022
Accepted 22 August 2022
Available online 28 August 2022

Keywords:
Lead-free
Hybrid halide double perovskites
Ferroelastics
Phase transition
Order-disorder

ABSTRACT

Ferroelastic materials with switchable spontaneous strain possess widely potential applications in the field of energy and information conversion. Recently, organic-inorganic hybrid halide double perovskites (OIHHDPs) have become a charming new platform for developing various functional materials, such as ferroelectrics, fluorescence and X–ray detection. Nevertheless, OIHHDP ferroelastic materials, especially high-temperature ones, are rare. Herein, we initially synthesized an OIHHDP ferroelastic, (2,2-difluoroethanamine)$_2$[$(NH_4)InCl_6$] (**1**), which possesses a ferroelastic phase transition at 407 K. Moreover, thanks to the flexible B-site for OIHHDPs, we replaced the NH_4^+ ions within $[(NH_4)InCl_6]_n^{2n-}$ formworks with K^+ ions, which endows with coordination bonds between 2,2-difluoroethanamine organic cations and $[KInCl_6]_n^{2n-}$ formworks. Due to the existence of coordination bonds, the phase transition temperature of (2,2-difluoroethanamine)$_2$[$KInCl_6$] (**2**) can reach 458 K. As far as we know, this value is the highest reported in OIHHDP ferroelastics. This work offers inspiration for the design of high-temperature OIHHDP phase transition materials including ferroelectrics and ferroelastics.

© 2023 Published by Elsevier B.V. on behalf of Chinese Chemical Society and Institute of Materia Medica, Chinese Academy of Medical Sciences.

Ferroelastic materials with spontaneous strain that can change under external stress possess wide applications, such as in data storage, sensors and mechanical switches [1–4]. Inorganic materials have been dominating the mainstream of ferroelastic materials, as exemplified by $BiVO_4$, $Pb_3(PO_4)_2$ and $LaAlO_3$ [5–7]. Nevertheless, they suffer from high-temperature processing, lack of mechanical flexibility and potential heavy metal toxicity. Molecule-based ferroelastic materials have become a competitive alternative to inorganic counterparts due to their advantages of solution processability, superior mechanical flexibility and environmental friendliness [8–10]. Among them, organic-inorganic hybrid halide perovskites (OIHHPs) have become an appealing playground for developing molecule-based ferroelastic materials due to structural tunability and variability [11,12]. Meanwhile, due to the multifunctionality of OIHHPs, substantial efforts have been devoted to exploring the coupling effect of ferroelasticity with other properties in these materials [13,14]. For instance, Centrone *et al.* demonstrated that the high-power conversion efficiency of $MAPbI_3$ solar cells is related to ferroelasticity [14]. Xiong *et al.* reported an OIHHP $TMCMMnCl_3$ with a large piezoelectric response comparable to $BaTiO_3$, ascribed to the multiaxial ferroelectricity in tandem with ferroelasticity [13].

Recently, organic-inorganic hybrid halide double perovskites (OIHHDPs), a class of novel materials, have attracted growing attention [15–17]. Theoretically, OIHHDPs outperform OIHHPs in terms of structural tunability and variability as their ions in the octahedral sites (B-site) consist of alternating monovalent ions and trivalent ions, implying a wider range of choices [18–21]. Meanwhile, OIHHDP materials have made gratifying achievements in developing functional materials [10,17,22,23]. For example, using *n*-propylammonium cations to slice inorganic three-dimensional (3D) $CsAgBiBr_7$, the first 2D OIHHDP ferroelectric material was obtained [24]. Sun *et al.* demonstrated the promising potential of OIHHDP materials in the field of X-ray detection [25]. Strong bright broadband emissions were discovered in 2D OIHHDP (phenethylamine)$_4NaInCl_8$:Sb and (phenethylamine)$_2CsNaInCl_7$:Sb [26]. Up to now, however, only a few OIHHDP ferroelastics have been reported, such as (*n*-butylammonium)$_2CsAgBiBr_7$ and (piperidinium)$_2$[$KBiCl_6$] [27,28]. Despite these achievements, how to improve the phase transition temperature of OIHHDP ferroelastic materials is an important problem to be solved since a high phase transition temperature means a high working temperature range which is a prominent parameter in the practical application for ferroelastic materi-

* Corresponding authors.
E-mail addresses: yizhang1980@seu.edu.cn (Y. Zhang), miaoleping@jxust.edu.cn (L.-P. Miao).

https://doi.org/10.1016/j.cclet.2022.107774
1001-8417/© 2023 Published by Elsevier B.V. on behalf of Chinese Chemical Society and Institute of Materia Medica, Chinese Academy of Medical Sciences.

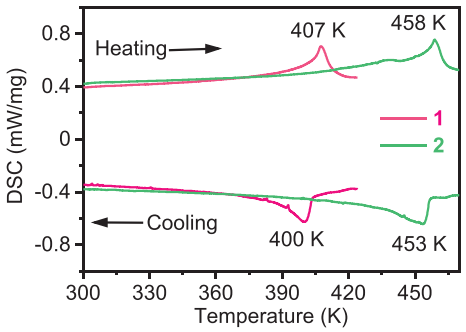

Fig. 1. DSC curves of **1** (red) and **2** (blue) in heating and cooling run.

als. Numerous proven and effective strategies have been developed to modulate the phase transition temperature of phase transition materials, such as strain engineering, isotope effect, fluorine substitution strategy [29–33]. Among them, the isotope effect has made great success, as exemplified by the relatively large phase transition temperature difference between $PbHPO_4$ (310 K) and $PbDPO_4$ (452 K); the fluorine substitution strategy has also achieved remarkable achievements in inducing ferroelectricity and enhancing phase transition temperature; the strain engineering is mainly suitable for inorganic materials [30,34–37].

In this context, we initially present a 1D OIHHDP ferroelastic, (2,2-difluoroethanamine)$_2$[$(NH_4)InCl_6$] (**1**), with a $\bar{3}mF2/m$ type of ferroelastic phase transition at 407 K. Further, by virtue of flexible B-site for OIHHDPs, we replaced the NH_4^+ ions within $[(NH_4)InCl_6]_n^{2n-}$ formworks with K^+ ions, resulting in that C–F···H hydrogen bonds between 2,2-difluoroethanamine organic cations and inorganic formworks are replaced with C–F–K coordination bonds (CBs). The introduction of CBs enables (2,2-difluoroethanamine)$_2$[$KInCl_6$] (**2**) to reach 458 K, which is 51 K higher than that of **1**, and possesses the same $\bar{3}mF2/m$ type of ferroelastic phase transition.

Colorless single crystals of **1** and **2** (Fig. S1 in Supporting information) were prepared by evaporating slowly the aqueous hydrochloric acid solution containing stoichiometric amounts of 2,2-difluoroethanamine, $InCl_3$ and NH_4Cl (**1**) or KCl (**2**) (details can be seen in Supporting information). The powder X-ray diffraction (PXRD) measurements were carried out to verify phase purity of **1** and **2**. As shown in Fig. S2 (Supporting information), the experimental PXRD patterns of **1** and **2** are in line with calculated counterparts based on the single-crystal structure information at 301 K, suggesting that the phases of **1** and **2** are pure.

Differential scanning calorimetry (DSC) measurements were adopted to detect phase transition temperature for **1** and **2**. As shown in Fig. 1, the DSC curve (red) of **1** exhibits separately an endothermic and exothermic peak at 407 and 400 K in heating and cooling run, indicating a reversible phase transition. Notably, after NH_4^+/K^+-substitution was carried out, DSC curve (blue) of **2** presents a pair of reversible thermal anomalies at 458 K (heating run) and 453 K (cooling run). The phase transition temperature of **2** is 51 K higher than that of **1**, suggesting that NH_4^+/K^+-substitution really increases phase transition temperature. The enthalpy change (ΔH) and entropy changes (ΔS) of **1** and **2** were calculated separately to be about 3.45 kJ/mol, 8.48 J mol^{-1} K^{-1} and 2.99 kJ/mol, 6.53 J mol^{-1} K^{-1}, implying that **1** and **2** possess a first-order phase transition.[38] According to the Boltzmann equation ($\Delta S = R\ln N$, where R is gas constant, N is the ratio of possible configurations, details can be seen in Supporting information), the N of **1** and **2** was estimated to be 2.78 and 2.2, respectively, which is greater than 2, suggesting an order-disorder phase transition feature [39]. The relatively large thermal hysteresis of **1** (7 K) and **2** (5 K) suggests a first-order phase transition [40]. For convenience,

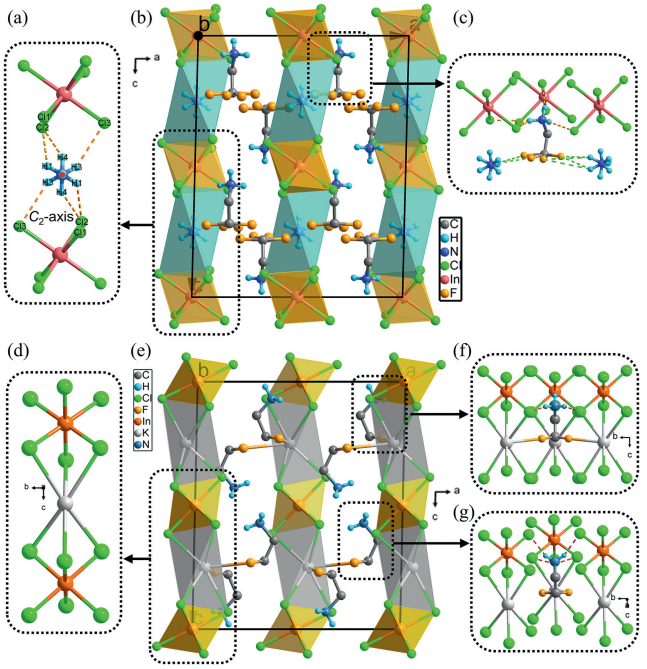

Fig. 2. (a) Disordered NH_4^+ ion within $[(NH_4)InCl_6]_n^{2n-}$ formworks. (b) Packing diagram of **1** along b axis in LTP. (c) Hydrogen bond distribution of 2,2-difluoroethanamine cation in **1**. (d) $[KInCl_6]_n^{2n-}$ formworks in **2**. (e) Packing diagram of **2** along b axis in LTP. Two 2,2-difluoroethanamine organic cations in different configurations: (f) two F atoms of 2,2-difluoroethanamine organic cations coordinated with the different K^+ ions, namely form A, and (g) two F atoms of 2,2-difluoroethanamine organic cations coordinated with the same a K^+ ions, namely form B. The H atoms of C atoms were omitted for clarity.

we labeled the phase above and below the phase transition temperature (407 K for **1** and 458 K for **2**) as high-temperature phase (HTP) and low-temperature phase (LTP), respectively.

Variable-temperature single-crystal X-ray diffraction measurements were performed to investigate the phase transition mechanism of **1** and **2**, and the effect of NH_4^+/K^+-substitution. In LTP, **1** crystallizes in the monoclinic space group of $C2/c$ (point group $2/m$) with a cell parameter: $a = 13.0539(3)$ Å, $b = 7.7268(2)$ Å, $c = 16.2067(4)$ Å, $\beta = 91.419(2)$ ° and $V = 1634.19(7)$ Å^3 (Table S1 in Supporting information). **1** adopts a hexagonal double perovskite structure, in which $InCl_6$ and $(NH_4)Cl_6$ octahedra adopting face-sharing mode construct 1D frameworks extending infinitely along c axis. Detailly, each In^{3+} ion is coordinated with six Cl^- ions to form $InCl_6$ octahedra, the In–Cl bond length ranging from 2.512 Å to 2.527 Å (Fig. S3a in Supporting information); each NH_4^+ ion interacts with the surrounding six Cl^- ions by N–H···Cl hydrogen bonds and ionic bonds to form $(NH_4)Cl_6$ octahedra, in which NH_4^+ ions site the two-fold (C_2) rotation axis parallel to crystallography b axis, exhibiting two-fold disorder state (Figs. 2a and b) [28,41]. Thinking of NH_4^+ ion as one N^+ ion, the N–Cl bond length ranges from 3.311 Å to 3.39 Å (Fig. S3b in Supporting information). The distortion index (Δd) and bond angle variance (σ^2) were adopted to evaluate the distortion of individual $InCl_6$ and $(NH_4)Cl_6$ octahedra (detailed calculation process can be seen in Supporting information) [42]. As shown in Table S2 (Supporting information), the $\Delta d/\sigma^2$ for $(NH_4)Cl_6$ octahedra and $InCl_6$ octahedra in the **1** were calculated to be $9.79 \times 10^{-3}/751.47^{\circ 2}$ and $2.09 \times 10^{-3}/1.6427^{\circ 2}$, respectively, indicating that $(NH_4)Cl_6$ octahedra possess a worse distortion than that of $InCl_6$ octahedra. 2,2-Difluoroethanamine organic cations whose two F atoms of $-CF_2$ groups exhibit a disordered state with splitting into two parts occupy spaces among the 1D $[(NH_4)InCl_6]_n^{2n-}$ formworks. The in-

teractive forces between 2,2-difluoroethanamine organic cations and $[NH_4InCl_6]_n^{2n-}$ formworks mainly result from two aspects: N-H···Cl hydrogen bonds between $-NH_3^+$ groups and Cl^- ions of $[NH_4InCl_6]_n^{2n-}$ formworks; N-H···F hydrogen bonds between two F atoms of $-CF_2$ groups and NH_4^+ ions of 1D $[(NH_4)InCl_6]_n^{2n-}$ formworks (Fig. 2c). As shown in Fig. 2e, similar to **1**, **2** also adopts a 1D hexagonal double perovskite structure, and crystallizes in the monoclinic space group of $C2/m$ (point group $2/m$) with a cell parameter: $a = 13.3593(3)$ Å, $b = 7.5390(2)$ Å, $c = 15.9426(4)$ Å, $\beta = 91.246(2)$ ° and $V = 1605.29(7)$ Å^3 in LTP (Table S1). Different from **1**, 1D inorganic frameworks of **2** are composed of $InCl_6$ and KCl_6 octahedra connected to each other in a face-sharing mode (Fig. 2d). Similarly, the distortion of individual $InCl_6$ and KCl_6 octahedra in the **2** was evaluated by Δd and σ^2 (detailed calculation process can be seen in Supporting information). The $\Delta d/\sigma^2$ for $InCl_6$ and KCl_6 octahedra were $1.80 \times 10^{-3}/0.7846^{\circ 2}$ and $1.869 \times 10^{-2}/738.40^{\circ 2}$, respectively, suggesting $InCl_6$ octahedra possess more perfect octahedral configuration than that of KCl_6 octahedra. As NH_4^+ ions are replaced by K^+ ions, the interactive forces between two F atoms of $-CF_2$ groups and inorganic formworks changes from N-H···F hydrogen bonds to C–F–K CBs (Figs. 2f and g). Accordingly, 2,2-difluoroethanamine organic cations become ordered due to the existence of C–F–K CBs.

In HTP, both **1** and **2** transition to trigonal space group of $P\bar{3}m1$ (point group $\bar{3}m$) (Table S1). As shown in Fig. S4 (Supporting information), the relationship of lattice cell for **1** and **2** between LTP and HTP is $2a^{HTP} \approx a^{LTP} + b^{LTP}$, $b^{HTP} \approx b^{LTP}$, $2c^{HTP} \approx c^{LTP}$. 2,2-Difluoroethanamine organic cations of both **1** and **2** exhibit a disordered state, which site at 3-fold axis (C_3) and mirror plane (σ_v) (Figs. S5 and S6 in Supporting information). Therefore, the reversible phase transition of **1** and **2** mainly results from disordered rotating movement of 2,2-difluoroethanamine organic cations. The C–F–K CBs between organic cations and inorganic formworks raise the potential rotating energy barrier of organic cations, which in turn increases the phase transition temperature of **2**. Similar examples have been reported [43,44].

To understand the C–F–K CBs generating intermolecular interactions between the cations and inorganic formworks, we obtained the visualization map of the distribution of the interactions by Hirshfeld surface analysis [45–48]. For Hirshfeld surface of **1**, the blue and white areas are predominant, and the red areas focus on the hydrogen bonding interactions [F···H] and [H···Cl]. The 2D fingerprint plots showing [F···H] and [H···Cl] interactions are 19.3% (Fig. S7 in Supporting information) and [H···Cl] 44.2% (Fig. 3a), respectively. Although the [F···F] interaction shows a red area and the interaction is 12.6%, the result is pseudo that the repelling interaction of F atoms is caused by the disordered treatment. As for crystal **2**, the red areas of the surfaces of F atom and H atoms are increased, showing stronger molecular interaction. The 2D fingerprint plots showing the two [H···Cl] interactions are 47.4% (A), 43.6% (B), respectively (Figs. 3b and c). Moreover, C–F–K CB ([F···K]) also shows red areas, and the 2D fingerprint plots of [F···K] interaction show the interactions are 8.0% (A), 4.5% (B), respectively (Fig. S8, Supporting information). Therefore, the Hirshfeld surface analysis reveals the C–F–K CBs certainly enhance the interactions between the cations and inorganic frameworks, and then increase the rotating energy barrier of the cations and anions. This result corresponds to the DSC measurement that the phase transition temperature of **2** increased substantially comparing with **1**.

The reversible phase transition of crystals usually goes with dielectric constant anomalies [49,50]. We recorded the real part of complex dielectric constant (ε', $\varepsilon = \varepsilon' - i\varepsilon''$, where ε is the complex dielectric constant; ε'' is the imaginary part) of **1** and **2** dependent on the temperature variation. As shown in Fig. 4a, the ε' of **1** exhibits a gradual increase as the temperature rises. When the temperature increases to around phase transition temperature

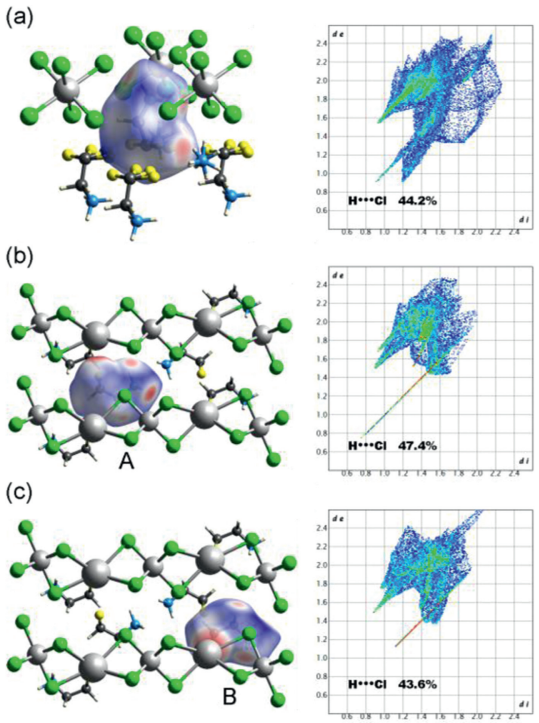

Fig. 3. The Hirshfeld surfaces mapped with d_{norm} and fingerprint plots for 2,2-difluoroethanamine organic cations of **1** in (a) LTP, and 2,2-difluoroethanamine organic cations in (b) form A and (c) B of **2** in LTP.

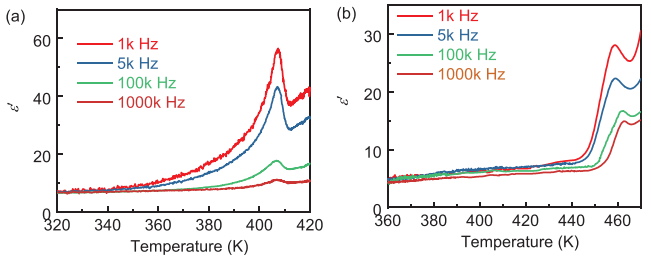

Fig. 4. The ε' of (a) **1** and (b) **2** as a function of temperature.

(407 K), the large dielectric anomalies can be observed within the frequency of 1-1000 kHz. The highest value of ε' for the frequency of 500 Hz is 8 times than that of one at the stable state, confirming that **1** possesses a phase transition. As shown in Fig. 4b, the ε' of **2** below around 458 K exhibits a stable state of about 6. As temperature rises to 458 K, the ε' of **2** presents a spike, suggesting a phase transition. Moreover, with increase of temperature, the ε'' of **1** and **2** also presents anomalies at about 407 and 458 K, respectively (Fig. S9 in Supporting information). The variable-temperature ε' and ε'' measurements further confirm an increase of phase transition temperature after NH_4^+/K^+-substitution, in line with the results of DSC measurements.

According to Aizu notation, both **1** and **2** undergo a $\bar{3}mF2/m$ type of ferroelastic phase transition [51]. The number of symmetry elements change from 12 (E, $2C_3$, $3C_2$, i, $2S_6$ and $3\sigma_v$) in HTP to four (E, C_2, i and σ_h) in LTP, and therefore spontaneous strain of both **1** and **2** possesses three possible orientation states. Ferroelastic domains with different orientation strains exhibit different birefringence properties under orthogonally polarized light [8,52]. Therefore, ferroelastic domains can be observed based on this theory with the polarized optical microscope. Adopting orthogonally polarized light with transmission mode, the evolution of ferroelastic domain structure for single-crystal of **1** was observed from

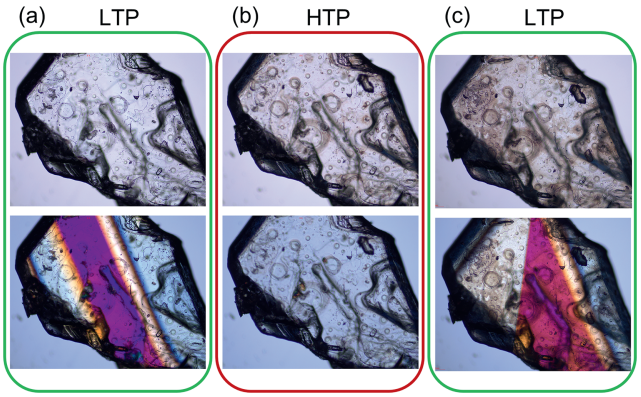

Fig. 5. Evolution of the ferroelastic domain structure for **1** from (a) LTP to (b) HTP to (c) LTP. The first and second column panels represent natural and optical polarized microscope images for single-crystal of **1**, respectively.

LTP to HTP to LTP. As shown in the second column panels of Fig. 5a, the single-crystal of **1** presents distinct stripe ferroelastic domains in LTP. As the temperature increases to above 407 K (HTP), the single-crystal of **1** exhibits uniform contrast, suggesting that ferroelastic domains disappear (Fig. 5b). As the single-crystal of **1** back to low 407 K (LTP), the ferroelastic domains reappear and change, implying a reversible ferroelastic transition phase (Fig. 5c). Additionally, a group of natural optical microscope images *in situ* for single-crystal of **1** was obtained as a control to eliminate the possibility of different birefringence effects from the interference of morphology of single-crystal. As shown in first column panels of Fig. 5, there is no relationship between ferroelastic domains and the morphology of single-crystal. As shown in Fig. S10 (Supporting information), the evolution of the ferroelastic domain structure for **2** from LTP to HTP to LTP can be also observed, confirming its ferroelasticity.

In summary, we presented two one-dimensional high-temperature organic-inorganic hybrid halide double perovskite (OIHHDP) ferroelastic materials, (2,2-difluoroethanamine)$_2$[$(NH_4)InCl_6$] (**1**) and (2,2-difluoroethanamine)$_2$[$KInCl_6$] (**2**). **1** possesses a high phase transition temperature of 407 K. **2** exhibits a higher phase transition temperature of 458 K, due to the existence of C–F–K CBs between 2,2-difluoroethanamine organic cations and $[KInCl_6]_n^{2n-}$ formworks. The evolution of ferroelastic domains for **1** and **2** was observed by the polarized optical microscope. This work sheds light on the design of eco-friendly high-temperature OIHHDP phase transition materials including ferroelectrics and ferroelastics.

Declaration of competing interest

The authors declare that they have no known competing financial interests or personal relationships that could have appeared to influence the work reported in this paper.

Acknowledgments

This work was supported financially by the National Key Research and Development Program of China (No. 2017YFA0204800), National Natural Science Foundation of China (Nos. 22175079 and 21875093), Natural Science Foundation of Jiangxi Province (Nos. 20204BCJ22015 and 20202ACBL203001), Jiangxi Provincial Department of Education Science and Technology Research Project (No. GJJ210812).

Supplementary materials

Supplementary material associated with this article can be found, in the online version, at doi:10.1016/j.cclet.2022.107774.

References

[1] D.X. Liu, Z.H. Yu, X.X. Chen, et al., Chin. Chem. Lett. 34 (2023) 107310.
[2] M.D. Hollingsworth, M.L. Peterson, K.L. Pate, et al., J. Am. Chem. Soc. 124 (2002) 2094–2095.
[3] A.I. Khan, X. Marti, C. Serrao, et al., Nano Lett. 15 (2015) 2229–2234.
[4] E.K.H. Salje, Annu. Rev. Mater. Res. 42 (2012) 265–283.
[5] H. Yokota, S. Matsumoto, E.K.H. Salje, et al., Phys. Rev. B 98 (2018) 104105–104111.
[6] C. Hill, M.C. Weber, J. Lehmann, et al., APL Mater. 8 (2020) 081108.
[7] H. Yokota, S. Niki, R. Haumont, et al., AIP Adv. 7 (2017) 085315.
[8] H.Y. Zhang, C.L. Hu, Z.B. Hu, et al., J. Am. Chem. Soc. 142 (2020) 3240–3245.
[9] M.M. Zhao, L. Zhou, P.P. Shi, et al., Chem. Eur. J. 25 (2019) 6447–6454.
[10] C.F. Wang, C. Shi, A. Zheng, et al., Mater. Horiz. 9 (2022) 2450–2459.
[11] S. Liu, L. He, Y. Wang, et al., Chin. Chem. Lett. 33 (2022) 1032–1036.
[12] Y.Y. Chen, C.H. Gao, T. Yang, et al., Chin. J. Struct. Chem. 41 (2022) 2204001–22040011.
[13] Y.M. You, W.Q. Liao, D. Zhao, et al., Science 357 (2017) 306–309.
[14] E. Strelcov, Q. Dong, T. Li, et al., Sci. Adv. 3 (2017) e1602165.
[15] Q. Jia, T. Shao, L. Tong, et al., Chin. Chem. Lett. 34 (2023) 107539.
[16] C. Su, Z. Zhang, J. Yao, et al., Chin. Chem. Lett. 34 (2023) 107442.
[17] D. Li, X. Liu, W. Wu, et al., Angew. Chem. Int. Ed. 60 (2021) 8415–8418.
[18] L. Mao, S.M.L. Teicher, C.C. Stoumpos, et al., J. Am. Chem. Soc. 141 (2019) 19099–19109.
[19] P. Vishnoi, J.L. Zuo, X. Li, et al., J. Am. Chem. Soc. 144 (2022) 6661–6666.
[20] F. Schmitz, J. Horn, N. Dengo, et al., Chem. Mater. 33 (2021) 4688–4700.
[21] C.F. Wang, H. Li, Q. Ji, et al., Adv. Funct. Mater. 32 (2022) 2205918.
[22] B. Vargas, G. Rodrıǵuez-López, D. Solis-Ibarra, ACS Energy Lett. 5 (2020) 3591–3608.
[23] C.F. Wang, H. Li, M.G. Li, et al., Adv. Funct. Mater. 31 (2021) 2009457.
[24] W. Zhang, M. Hong, J. Luo, Angew. Chem. Int. Ed. 59 (2020) 9305–9308.
[25] Z. Xu, X. Liu, Y. Li, et al., Angew. Chem. Int. Ed. 58 (2019) 15757–15761.
[26] Y. Zhang, X. Liu, H. Sun, et al., Angew. Chem. Int. Ed. 60 (2021) 7587–7592.
[27] X. Liu, Z. Xu, P. Long, et al., Chem. Mater. 32 (2020) 8965–8970.
[28] Q.R. Meng, W.J. Xu, W.H. Hu, et al., Chem. Commun. 57 (2021) 6292–6295.
[29] M. Itoh, R. Wang, Y. Inaguma, et al., Phys. Rev. Lett. 82 (1999) 3540–3543.
[30] K. Chang, J. Liu, H. Lin, et al., Science 353 (2016) 274–278.
[31] Y. Ai, H.P. Lv, Z.X. Wang, et al., Trend. Chem. 3 (2021) 1088–1099.
[32] B.D. Liang, T. Jin, L.P. Miao, et al., Chin. Chem. Lett. 33 (2022) 1422–1424.
[33] S. Koval, J. Kohanoff, R.L. Migoni, et al., Phys. Rev. Lett. 89 (2002) 187602–187606.
[34] T.J. Negran, A.M. Glass, C.S. Brickenkamp, et al., Ferroelectrics 6 (1973) 179–182.
[35] Y. Ai, X.G. Chen, P.P. Shi, et al., J. Am. Chem. Soc. 141 (2019) 4474–4479.
[36] P.P. Shi, S.Q. Lu, X.J. Song, et al., J. Am. Chem. Soc. 141 (2019) 18334–18340.
[37] Z.X. Wang, Y. Zhang, Y.Y. Tang, et al., J. Am. Chem. Soc. 141 (2019) 4372–4378.
[38] Y.L. Zeng, X.Q. Huang, C.R. Huang, et al., Angew. Chem. Int. Ed. 60 (2021) 10730–10735.
[39] Z. Sun, Y. Tang, S. Zhang, et al., Adv. Mater. 27 (2015) 4795–4801.
[40] Y.Y. Tang, Y. Ai, W.Q. Liao, et al., Adv. Mater. 31 (2019) 1902163.
[41] H.Y. Ye, Y.Y. Tang, P.F. Li, et al., Science 361 (2018) 151–155.
[42] K. Robinson, G.V. Gibbs, P.H. Ribbe, Science 172 (1971) 567–570.
[43] X.G. Chen, Z.X. Zhang, Y.L. Zeng, et al., Chem. Commun. 58 (2022) 3059–3062.
[44] W.J. Xu, P.F. Li, Y.Y. Tang, et al., J. Am. Chem. Soc. 139 (2017) 6369–6375.
[45] M.A. Spackman, J.J. McKinnon, CrystEngComm 4 (2002) 378–392.
[46] M.A. Spackman, D. Jayatilaka, CrystEngComm 11 (2009) 19–32.
[47] Q. Xu, L. Ye, R.M. Liao, et al., Chem. Eur. J. 28 (2022) e202103913.
[48] P.R. Spackman, M.J. Turner, J.J. McKinnon, et al., J. Appl. Crystallogr. 54 (2021) 1006–1011.
[49] Y. Xue, Z. Zhang, P. Shi, et al., Chin. Chem. Lett. 32 (2021) 539–542.
[50] M.A. Asghar, J. Zhang, S. Han, et al., Chin. Chem. Lett. 29 (2018) 285–288.
[51] K. Aizu, J. Phys. Soc. Jpn. 27 (1969) 387–396.
[52] W.J. Xu, Y. Zeng, W. Yuan, et al., Chem. Commun. 56 (2020) 10054–10057.